RESEARCH ARTICLE | MAY 08 2019

Probing and possible application of the QED vacuum with micro-bubble implosions induced by ultra-intense laser pulses

Special Collection: Special Issue on Extreme High-Field Physics Driven by Lasers

James K. Koga ; Masakatsu Murakami ; Alexey V. Arefiev ; Yoshihide Nakamiya

Matter Radiat. Extremes 4, 034401 (2019)
https://doi.org/10.1063/1.5086933

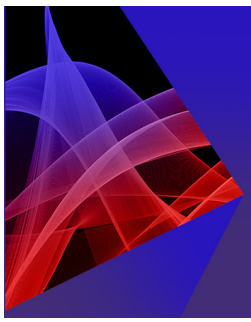

Matter and Radiation at Extremes | RESEARCH ARTICLE | scitation.org/journal/mre

Probing and possible application of the QED vacuum with micro-bubble implosions induced by ultra-intense laser pulses

Cite as: Matter Radiat. Extremes 4, 034401 (2019); doi: 10.1063/1.5086933
Submitted: 25 December 2018 • Accepted: 19 February 2019 •
Published Online: 8 May 2019

James K. Koga,[1] Masakatsu Murakami,[2] Alexey V. Arefiev,[3] and Yoshihide Nakamiya[4]

AFFILIATIONS

[1] Kansai Photon Science Institute, National Institutes for Quantum and Radiological Science and Technology, Kizugawa, Kyoto 619-0215, Japan
[2] Institute of Laser Engineering, Osaka University, Osaka 565-0871, Japan
[3] Department of Mechanical and Aerospace Engineering, University of California at San Diego, La Jolla, California 92093, USA
[4] Extreme Light Infrastructure-Nuclear Physics (ELI-NP)/Horia Hulubei National Institute for R&D in Physics and Nuclear Engineering (IFIN-HH), 30 Reactorului St., P.O. Box MG-6, Bucharest-Magurele, Judeţul Ilfov RO-077125, Romania

ABSTRACT

The interaction of micro-bubbles with ultra-intense laser pulses has been shown to generate ultra-high proton densities and correspondingly high electric fields. We investigate the possibility of using such a combination to study the fundamental physical phenomenon of vacuum polarization. With current or near-future laser systems, measurement of vacuum polarization via the bending of gamma rays that pass near imploded micro-bubbles may be possible. Since it is independent of photon energy to within the leading-order solution of the Heisenberg–Euler Lagrangian and the geometric optics approximation, the corresponding index of refraction can dominate the indices of refraction due to other effects at sufficiently high photon energies. We consider the possibility of its application to a transient gamma-ray lens.

I. INTRODUCTION

With the advent of ultra-high-power lasers of order 10 petawatts (PW)[1,2] and higher,[3] the possibility of studying the vacuum with such lasers has attracted a great deal of interest.[3,4] In the regime where vacuum polarization has been considered, most studies have concentrated on the effects of photons interacting with magnetic fields alone or with crossed electric and magnetic fields. Although the effect of the Coulomb field of a single nucleus on photon scattering (i.e., Delbrück scattering) has been studied extensively,[5,6] the effect of a macroscopic electric field has not received as much attention. This can be attributed to the fact that strong macroscopic electrostatic fields dissipate quickly owing to the presence of surrounding charges, whereas the situation is very different for magnetic fields because of the nonexistence (or exceeding rarity) of magnetic monopoles.[7] However, it should be noted that owing to the electric–magnetic duality of the Heisenberg–Euler effective Lagrangian that is used to describe the vacuum signatures of the quantum electrodynamic (QED) vacuum, nonlinearities in magnetic fields can be generically mapped to corresponding nonlinearlities in electric fields (see, e.g., Refs. 8 and 9). It has recently been proposed that very strong macroscopic electrostatic fields could be generated via micro-bubble implosions.[10] Using this approach, extremely high ion densities and thus unprecedented Coulomb fields should be achievable. In this paper, we show that, by using such micro-bubble implosions, vacuum polarization can be measured and also that such micro-bubbles could be considered as components of transient lenses for gamma rays.

II. PHOTON TRAJECTORY

The value of the electric field at which nonlinear QED effects are expected to occur is the Schwinger field E_S, given by[11–13]

$$E_S = \frac{m_e^2 c^3}{e\hbar} = 1.32\times10^{18}\ \mathrm{V/m}, \tag{1}$$

where m_e is the electron mass, c is the speed of light in vacuum, and $\hbar$ is Planck's constant divided by 2π. The electric field E_f of an imploding spherical micro-bubble at around the time of maximum compression is given by[10]

$$E_f(r) = \frac{Q_0}{2R_0 r}, \tag{2}$$

where r is the radius of the micro-bubble, R_0 is its initial radius, and Q_0 is the total electron charge in the initial bubble, which is equal to eN_{e0}, where $N_{e0} = (4\pi/3)R_0^3\tilde{n}_{e0}$, with $\tilde{n}_{e0}$ being the average electron density in the bubble and e the electron charge. The maximum field $E_{\max} = E_f(r_{\min})$ occurs on the surface of the imploded micro-bubble when the minimum radius $r_{\min}$ is attained. This minimum radius is given by[10] $r_{\min} = 3n_{i0}^{2/3}/\tilde{n}_{e0}$, where n_{i0} is the initial ion density. Taking the ratio of the Schwinger and maximum fields, we get

$$\frac{E_{\max}}{E_S} = \frac{2\pi}{9}\left(\frac{\tilde{n}_{e0}}{n_{i0}^{1/3}}\right)^2 R_0^2 r_e \lambda_e, \tag{3}$$

where the classical electron radius $r_e \equiv e^2/m_e c^2$ and the Compton wavelength $\lambda_e \equiv \hbar/m_e c$. From this, we can see that the important parameters governing the maximum field are $\tilde{n}_{e0}$, n_{i0}, and R_0. Using typical values of $n_{i0} = 5 \times 10^{22}$ cm^{-3}, $\tilde{n}_{e0} = 5 \times 10^{21}$ cm^{-3}, and $R_0 = 2$ μm from Ref. 10, we get $E_{\max}/E_S \approx 5.6 \times 10^{-3}$, and thus the maximum field is more than 0.5% of the Schwinger field (7.4×10^{15} V/m) with $r_{\min} = 8.14$ nm. Ultrahigh electric fields close to the Schwinger field (1) could be achieved at even higher laser intensities of $I_L \sim 10^{22}$ W/cm^2 together with an appropriate amount of invested laser energy, giving $r_{\min} \sim 1$ nm (see, e.g., Fig. 6 in Ref. 10) and subsequent electron–positron pair production. In this paper, we will concentrate on vacuum polarization.

To observe the effects on vacuum polarization, we propose the use of gamma rays traversing the imploding micro-bubble. The trajectory of light deflected due to vacuum polarization represented by the Heisenberg–Euler Lagrangian[12,13] for a spherically symmetric charged object has previously been calculated in the geometric optics approximation for astrophysical objects.[14] For a homogeneous magnetic field—and therefore equivalently for an electric field, given the electric–magnetic duality of the Heisenberg–Euler Lagrangian—it has been shown that this is justified even for photons with energies much greater than the electron rest mass energy for sufficiently weak fields.[15] Further details concerning this will be presented in Sec. III A. For a charged object centered at $x = y = z = 0$, a photon moving in the $+x$ direction in the x–y plane starting at $x = -\infty$ with initial conditions $y(-\infty) = b$ and $y'(-\infty) = 0$ (where the prime indicates the derivative with respect to x) has been shown to obey (Gaussian units)[16]

$$y'' = \frac{a\alpha^2 Q^2 \lambda_e^4}{90\pi\hbar c}\left(\frac{y}{r^6} - \frac{3y^3}{r^8}\right), \tag{4}$$

where Q is the total charge, $\alpha \equiv e^2/\hbar c$ is the fine-structure constant, b is the impact parameter, and $a = 8$ or 14 for photon polarization respectively parallel or perpendicular to the scattering plane, where "parallel" and "perpendicular" here refer to polarization of the gamma ray respectively in or perpendicular to the **k**–**E** plane, with **k** being the direction of propagation and **E** the external electric field direction. The geometry is shown in Fig. 1. The scattering plane is centered on the origin of the imploded charge sphere at $x = y = z = 0$. Incoming gamma rays with polarizations purely parallel or perpendicular to the scattering plane will have a mixture of both components if they have an initial $z \neq 0$ away from the scattering plane, since the electric field is

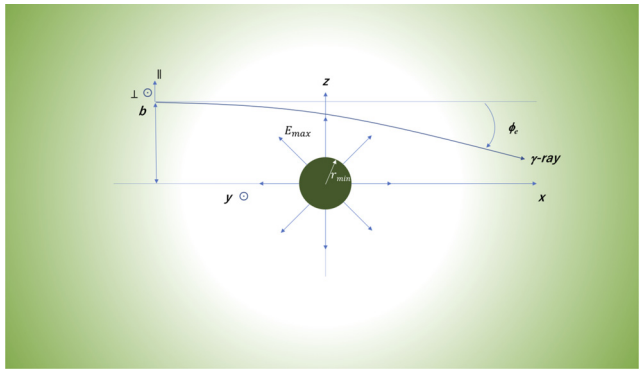

FIG. 1. Geometry of the interaction used in Ref. 14, where the imploded charged sphere is centered at $x = y = z = 0$, the scattering angle is ϕ_e, the impact parameter is b, and ∥ (parallel) and ⊥ (perpendicular) indicate the polarization of the incoming gamma ray, at the time at which $r_{\min}$ is the minimum radius, and $E_{\max}$ is the maximum electric field. The darker area around the core indicates the presence of the surrounding plasma.

radial. The deflection angle ϕ_e has been shown from the integration of Eq. (4) over x from $-\infty$ to ∞ to be (Gaussian units)[16]

$$y'(\infty) = \tan\phi_e = -\frac{a\alpha^2 Q^2}{160\hbar c}\left(\frac{\lambda_e}{b}\right)^4. \tag{5}$$

Re-expressing Eq. (5) in terms of R_0 and $\tilde{n}_{e0}$, we get

$$y'(\infty) = \tan\phi_e = -\frac{a\alpha^3}{160}\left(\frac{4\pi}{3}R_0^3\tilde{n}_{e0}\right)^2\left(\frac{\lambda_e}{b}\right)^4. \tag{6}$$

The typical value for $\tilde{n}_{e0}$ that we have chosen above is a variable and can be substantially greater, depending on the combination of laser and target parameters, owing to the fact that $\tilde{n}_{e0}$ is simply given by the total number of hot electrons produced divided by the limited target volume. Here, we examine the scattering angle over a range of $\tilde{n}_{e0}$, keeping R_0 fixed. In Fig. 2, we have plotted the absolute value of the scattering angle ϕ from Eq. (6) vs the impact parameter b over the range $r_{\min} \le b \le R_0$ for photon polarization parallel or perpendicular to the scattering plane, using the typical parameters from Ref. 10. Small differences exist between the cases with photon polarization parallel and perpendicular to the scattering plane for the same $\tilde{n}_{e0}$. However, they are not significant. In the figure, the index of refraction for $\tilde{n}_{e0} = 5 \times 10^{20}$ cm^{-3}, labeled by (0.1), stops at $b = 81.4$ nm because this is the smallest that $r_{\min}$ becomes for this case. Although the smallest $r_{\min}$ becomes 0.8 nm for $\tilde{n}_{e0} = 5 \times 10^{22}$ cm^{-3}, labeled by (10) in the figure, we have only plotted conservatively down to $b = 8.14$ nm, since below this value, the scattering angles become so large that the approximations may be violated (see the following paragraph). When the impact parameter b is close to $r_{\min}$ for the typical parameters, the scattering angles for perpendicular and parallel polarization are respectively -4.83×10^{-3} rad and -2.76×10^{-3} rad. Given that sub-nanoradian resolution is possible using devices such as GAMS6,[17] measurement of such scattering up to a few hundred nanometers away from the core is well within current technical capabilities. In Fig. 2, for $\tilde{n}_{e0} = 5 \times 10^{20}$ cm^{-3} [labeled by (0.1)] and 5×10^{22} cm^{-3} [labeled by (10)], the scattering angles for perpendicular and parallel polarization are respectively −0.485 rad and −0.277 rad at $b = 8.14$ nm, and -4.83×10^{-9} rad and -2.76×10^{-9} rad at $b = 81.4$ nm. For these

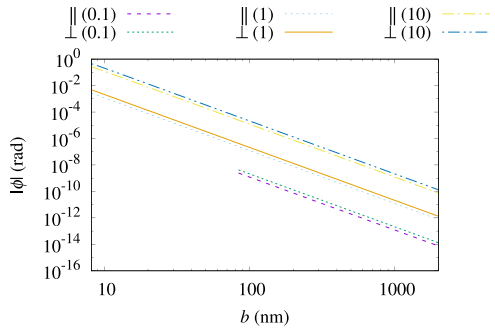

FIG. 2. Absolute value of the scattering angle ϕ from Eq. (6) vs the impact parameter b over the range $r_{min} \le b \le R_0$ for photon polarization parallel (||) or perpendicular (⊥) to the scattering plane and values of $\tilde{n}_{e0}$ equal to 5×10^{20} cm^{-3}, 5×10^{21} cm^{-3}, and 5×10^{22} cm^{-3}, labeled by (0.1), (1), and (10), respectively. Here, we have used $n_{i0} = 5 \times 10^{22}$ cm^{-3} and $R_0 = 2$ μm, with $r_{min} = 8.14$ nm for case (1).

values, the highest-density case produces easily measured large scattering angles, whereas in the lowest-density case, measurements are barely feasible, indicating that it is desirable to have $\tilde{n}_{e0} > 5 \times 10^{21}$ cm^{-3}.

We have calculated the maximum angles of scattering by vacuum polarization using Eq. (6), and the minimum radius of the micro-bubble, r_{min}, can be made very small by appropriate changes in $\tilde{n}_{e0}$, n_{i0}, and R_0. However, there is a limit to the applicability of the Heisenberg–Euler formalism for the vacuum, and so care must be taken when choosing the minimum impact parameter for the photon. The minimum value that we can choose for b in the Coulomb field is determined by the constraints that (1) the Heisenberg–Euler interaction is a small perturbation to Maxwell's equations and (2) the higher-order corrections to the Heisenberg–Euler interaction is small.[18] The first constraint is expressed by[18]

$$r_{\min\parallel,\perp}(1) \gg \lambda_e \left(\frac{aZ^2\alpha^3}{90}\right)^{1/4} \tag{7}$$

and the second by[18]

$$r_{\min}(2) \gg \sqrt{Z\alpha}\lambda_e, \tag{8}$$

where $r_{min||,\perp}(1)$ and $r_{min}(2)$ are the minimum radii for constraints (1) and (2), respectively, and $Z = N_e$. Using the range of parameters that we are considering, these constraints are given in Table I. For the lowest $\tilde{n}_{e0}$ case, $r_{min||,\perp}(1)$, $r_{min}(2) < r_{min}$. For the typical $\tilde{n}_{e0}$ case $r_{min||,\perp}(1) < r_{min} \lesssim r_{min}(2)$ where the main constraint is on the effect of higher order perturbations; however, r_{min} and $r_{min}(2)$ are of the same order. In the highest $\tilde{n}_{e0}$ case, $r_{min} < r_{min||,\perp}(1)$, $r_{min}(2)$, indicating that the paths of photons passing close to the imploded core need to be calculated in a different manner.

III. INDEX OF REFRACTION

In Sec. II, the bending of gamma rays was formulated using Eq. (6). This bending effect is interpreted as a consequence of an index of refraction of the vacuum induced by the micro-bubble implosion. Here, we evaluate the expected strength of this index of refraction and possible background processes such as plasma effects. For simplicity, we consider the typical parameters for the micro-bubble from Ref. 10.

TABLE I. Minimum impact parameter b allowed in the Heisenberg–Euler interaction for different values of $\tilde{n}_{e0}$, with $n_{i0} = 5 \times 10^{22}$ cm^{-3} and $R_0 = 2$ μm fixed, where || and ⊥ refer to polarization respectively perpendicular and parallel to the scattering plane, and "(1)" and "(2)" indicate the constraint number. r_{min} and E_{max}/E_S are also shown for comparison.

$\tilde{n}_{e0}$ (cm^{-3})	$r_{min||,\perp}(1)$ (nm)	$r_{min}(2)$ (nm)	r_{min} (nm)	E_{max}/E_S
5×10^{20}	(0.681, 0.784)	4.27	81.4	5.6×10^{-5}
5×10^{21}	(2.15, 2.48)	13.5	8.14	5.6×10^{-3}
5×10^{22}	(6.81, 7.84)	42.7	0.8	0.56

A. Vacuum polarization effects

The indices of refraction $n_{\parallel,\perp}$ of the vacuum from the Heisenberg–Euler Lagrangian for a homogeneous electrostatic field $\vec{E}$ are given in terms of E_S as follows (see, e.g., Ref. 16 and references therein):

$$n = 1 + \frac{a\alpha}{180\pi}\left(\frac{\vec{u}\times\vec{E}}{E_S}\right)^2, \tag{9}$$

where $\vec{u}$ is the unit vector in the direction of photon propagation. Using the typical parameters from above, taking $E/E_S = E_{max}/E_S \approx 5.6 \times 10^{-3}$, and assuming propagation perpendicular to the field, we find that $\delta_\parallel = n_\parallel - 1 = 3.2 \times 10^{-9}$ and $\delta_\perp = n_\perp - 1 = 5.6 \times 10^{-9}$. These values are of the order of those measured for gamma rays with photon energies between 517 keV and 1951 keV for a variety of elements.[17] The index of refraction of the polarized vacuum is independent of the photon energy to leading order using the Heisenberg–Euler Lagrangian.[19] Higher-order corrections do produce an energy dependence,[15,20,21] but, in the case of a homogeneous magnetic field, it has been shown that the index of refraction is still given by Eq. (9) provided that $\xi \ll 1$, where $\xi \equiv \frac{3}{2}[\hbar\omega/(mc^2)](H/H_{cr})$.[15] Since $H_{cr} = E_S$, H/H_{cr} is equivalent to E/E_S. Given that for the above parameters, $E_{max}/E_S \approx 5.6 \times 10^{-3}$ at photon energies below 60 MeV, this is maintained. These photon energies will be lower or higher, depending on whether the initial total electron charge $N_{e0} \propto R_0^3 \tilde{n}_{e0}$, which determines the maximum electric field, is higher or lower, respectively. For higher photon energies or stronger fields, solutions exist that can be used when studying these regimes (see Ref. 9 and references therein or Ref. 15).

B. Plasma effects

Since the micro-bubble implosion occurs in a plasma, the effects of the plasma on gamma-ray propagation should be taken into account. The effect on the index of refraction n due to vacuum polarization has previously been taken into account for a cold plasma with a background magnetic field:[20]

$$n = 1 - \frac{1}{2}\left(\frac{\omega_p}{\omega_\gamma}\right)^2, \tag{10}$$

where $\omega_p = \sqrt{4\pi e^2 n_p/m_e}$, n_p is the plasma density, and $E_\gamma = \hbar\omega_\gamma$. Taking the surrounding plasma density $n_p = n_{i0} = 5 \times 10^{22}$ cm^{-3}, the equivalent energy is $E_p = \hbar\omega_p = 8.3$ eV. We can see that $\delta = n - 1$ will be smaller than the values calculated for vacuum refraction when the gamma-ray energies are above a few hundred kiloelectron volts. Relativistically hot plasmas having an electron temperature anisotropy normally occur in the interaction of ultrahigh-intensity lasers

with targets, as a result of which the propagation of laser light varies, depending on the anisotropy.[22,23] The main point we wish to make here is that in a relativistic plasma, the ratio $(\omega_p/\omega_\gamma)^2$ is further reduced by γ, the relativistic gamma factor of the relativistically hot plasma, decreasing the effect of the plasma on the total index of refraction. Since the effects are smaller in the hotter direction of an anisotropic relativistic-temperature plasma,[22,23] further optimization could be done by an appropriate choice of the gamma-ray polarization direction with respect to the anisotropy.

C. Other effects

In addition to the effects of the plasma, we should also consider other effects in the interaction of gamma rays with solid materials. These have been estimated in Ref. 17. The index of refraction can be written as[17]

$$n(E_\gamma) = 1 + 2\pi\frac{(\hbar c)^2}{E_\gamma^2}\sum_k N_k A_k(E_\gamma, 0), \tag{11}$$

where E_γ is the photon energy, the sum is over the types of atoms, k, N_k is the number of atoms of type k per unit volume, and A_k is the forward scattering amplitude for atoms of type k. The elastic scattering amplitudes are sums of the amplitudes for nuclear Thomson scattering, Rayleigh scattering by bound electrons, Delbrück scattering, and nuclear resonance scattering.[17,24] Since our example is for hydrogen, we will ignore nuclear resonance scattering. The nuclear Thomson scattering amplitude is given by[17,25]

$$A_T(E_\gamma, 0) = -Z^2 r_e \frac{m_e}{M}, \tag{12}$$

where Z is the atomic charge number and M is the mass of the nucleus. The Rayleigh scattering amplitude can be approximated by considering the scattering of Z free electrons (classical approximation):[17]

$$A_R(E_\gamma, 0) = -Zr_e. \tag{13}$$

In the case of the micro-bubble implosion, the hydrogen atoms are assumed to be fully ionized. As a result, this component becomes equivalent to the cold plasma contribution and is therefore neglected here. The Delbrück scattering amplitude in the Born approximation is as follows (with $\omega \equiv E_\gamma/m_e c^2$):[26] for $E_\gamma < 4m_e c^2$,

$$A_D(E_\gamma, 0) = (\alpha Z)^2 r_e (B_1\omega^2 + B_2\omega^4 + B_3\omega^6), \tag{14}$$

where $B_1 = 3.1735 \times 10^{-2}$, $B_2 = 3.1610 \times 10^{-4}$, and $B_3 = 1.4790 \times 10^{-5}$; for $E_\gamma > 4m_e c^2$,

$$A_D(E_\gamma, 0) = (\alpha Z)^2 r_e\left(\frac{7}{18}\omega + A_1 + \frac{\ln^2\omega}{\omega} + A_2\frac{\ln\omega}{\omega} + \frac{A_3}{\omega} + \frac{A_4}{\omega^2} - \frac{3}{8\omega^3} + \frac{A_5}{\omega^4} - \frac{29}{288\omega^5} + \frac{A_6}{\omega^6}\right), \tag{15}$$

where $A_1 = -2.2512$, $A_2 = 0.38629$, $A_3 = 2.7873$, $A_4 = -3.5098$, $A_5 = 0.77$, and $A_6 = 3.6910$. The values of N_k depend on the scattering process. In the case of Rayleigh scattering, the largest contribution will be from the initial background electron density of $n_p = n_{i0} = 5 \times 10^{22}$ cm^{-3}. In the cases of nuclear Thomson scattering and Delbrück scattering, the maximum values are expected to be at the core, where the maximum core ion density $n_{\max}$ is given by[10]

$$\frac{n_{\max}}{n_{i0}} = \left(\frac{N_{e0}}{6^{7/2}\pi}\right)^{2/3}, \tag{16}$$

giving $n_{\max} \approx 10^{28}$ cm^{-3} with the typical parameters of Ref. 10. Figure 3 shows the contributions to the absolute value of the index of refraction, $\delta = n - 1$, from vacuum polarization ($\delta_\parallel$ and $\delta_\perp$) [using Eq. (9)], from nuclear Thomson and Delbrück scattering [using Eqs. (11), (12), (14), and (15)], and from plasma effects [using Eq. (10)] vs the normalized photon energy $E_\gamma/m_e c^2$. Parameter values of $n_p = 5 \times 10^{22}$ cm^{-3}, $Z = 1$, and $M/m_e = 1836.15267389$ have been chosen. We have plotted the index of refraction for photon energies in the regime where the vacuum polarization contribution is expected to be energy-independent. We can see that the vacuum contributions to the index of refraction are much larger than the other contributions for photon energies above a few megaelectron volts. By the time the photon energies are tens of megaelectron volts, the other contributions are about three orders of magnitude smaller. This means that for photon energies in this range, the vacuum polarization effect can be dominant and the trajectories calculated in Sec. II are valid.

D. Absorption processes

In the above calculations of the index of refraction, we have not considered the imaginary part, which represents absorption processes. Here, we briefly estimate this part for each component.

The contribution to the imaginary part of the index of refraction from vacuum polarization due to pair creation has been shown to be zero in pure magnetic fields and nonzero in static electric fields[27] (see also the review in Ref. 28). The vacuum has been shown to exhibit dichroism; that is, there is a preferential absorption of photons with polarization parallel vs perpendicular to the electric field.[27] The imaginary parts of the perpendicular, $\Im(n_\perp)$, and parallel, $\Im(n_\parallel)$, indices of refraction have been shown to have the forms[29]

$$\Im(n_\perp) = \frac{\alpha}{4\pi}\sin^2\theta\left[\frac{2}{3}\pi\left(e^{\pi/y} - 1\right)^{-1} - \frac{1}{y}\ln\left(1 - e^{-\pi/y}\right) + \frac{2}{\pi}e^{-\pi/y}{}_{1,1,1}F_{2,2}\left(e^{-\pi/y}\right) + \mathcal{O}\left(\left(\frac{\alpha}{4\pi}\right)^2\right)\right], \tag{17}$$

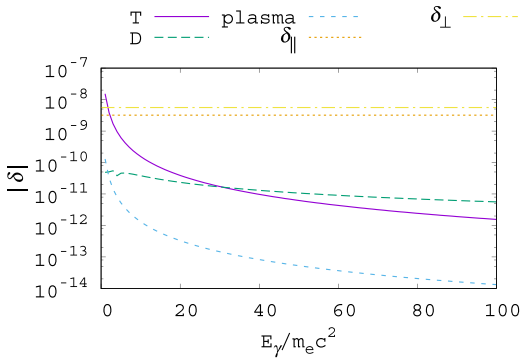

FIG. 3. Contributions to the absolute value of the index of refraction, $\delta = n - 1$, from vacuum polarization ($\delta_\parallel$ and $\delta_\perp$), nuclear Thomson scattering ("T"), Delbrück scattering ("D"), and plasma effects ("plasma") vs normalized photon energy $E_\gamma/m_e c^2$ (see the text for parameter values).

$$\Im(n_\parallel) = \frac{\alpha}{4\pi}\sin^2\theta\left[\frac{\pi}{y^2}\left(e^{\pi/y}-1\right)^{-1} - \frac{1}{y}\ln\left(1-e^{-\pi/y}\right) + \mathcal{O}\left(\left(\frac{\alpha}{4\pi}\right)^2\right)\right], \tag{18}$$

where θ is the angle between the direction of propagation and the external field, $y \equiv E/E_S$, and $F_{2,2}$ is a generalized hypergeometric function. With $y = E/E_S = E_{max}/E_S \approx 5.6 \times 10^{-3}$, both the perpendicular and parallel imaginary indices of refraction have arguments in their exponents of $\pi/y \sim 560$, implying that they are exceedingly small and can be neglected.

The plasma contribution to the imaginary part of the index of refraction in a cold plasma is significant only when the photon energy is below $E_p = \hbar\omega_p = 8.3$ eV. Therefore, since we are considering only high-energy photons, this contribution can be ignored.

The contribution of the individual atoms to the imaginary part of the index of refraction, $\beta(E_\gamma)$, is given by[17]

$$\beta(E_\gamma) = \sigma_{tot}(E_\gamma) N_{atom} \frac{\hbar c}{2E_\gamma}, \tag{19}$$

where σ_{tot} and N_{atom} are the total photo-absorption cross section and the atomic number density, respectively. The values of σ_{tot} can be obtained from the XCOM database, where the effects of incoherent scattering (Compton), coherent scattering (Rayleigh), photoelectric absorption, and pair production in the field of the atomic nucleus (electron–positron pairs) and in the field of the atomic electrons are taken into account.[30] Since the hydrogen is expected to be fully ionized, we neglect coherent scattering (Rayleigh) and photoelectric absorption. The number densities N_{atom} will be different for each process, as in Sec. III C. For the incoherent scattering and pair production in the field of the atomic electrons, we take the surrounding plasma density $n_p = n_{i0} = 5 \times 10^{22}$ cm^{-3}, and for the pair production in the field of the atomic nucleus, we take the maximum compression density $n_{max} \approx 10^{28}$ cm^{-3}. It should be noted that the pair production in the field of the atomic electrons takes into account various effects assuming initially bound electrons,[31] and we use it as an estimate. The values of $\beta(E_\gamma)$ are plotted for each component in Fig. 4. We have also plotted the real parts of the index of refraction, $\delta = n - 1$, due to vacuum polarization ($\delta_\parallel$ and $\delta_\perp$) for comparison. For our values of the parameters, it can be seen that at photon energies of 10 MeV and above, the largest contribution to the imaginary part of the index of refraction comes from pair production in the atomic nuclear field. The real parts of the index of refraction due to vacuum polarization are about two orders of magnitude larger than this.

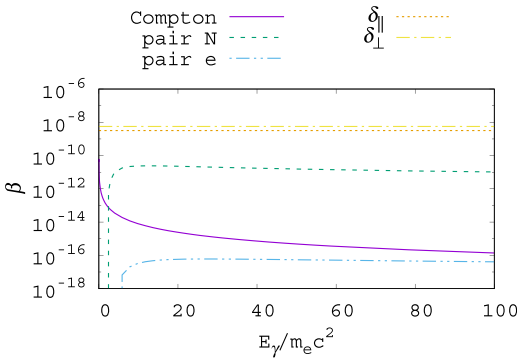

FIG. 4. Imaginary part of the index of refraction, $\beta(E_\gamma)$, obtained using values of σ_{tot} from the XCOM database,[30] vs normalized photon energy E_γ/m_ec^2. "Compton" refers to incoherent scattering, "pair N" to pair production in the atomic nuclear field, and "pair e" to pair production in the atomic electron field. The real parts of the index of refraction, $\delta = n - 1$, due to vacuum polarization ($\delta_\parallel$ and $\delta_\perp$) are also plotted for comparison.

In addition, there is a contribution from photon splitting, for which the following analytical fit to the cross section for an unscreened nucleus, $\sigma_{unscr}(E_\gamma)$, has been obtained:[32]

$$\sigma_{unscr} = Z^2\left(2.2372\ln\omega - 4.7313 + \frac{8.2536}{\omega} - \frac{3.164}{\omega^2}\right)\times 10^{-8}\ \text{b}, \tag{20}$$

where ω is the same as defined previously and $1\ \text{b} \equiv 10^{-24}\ \text{cm}^2$. Figure 5 shows a comparison between the absorption from photon splitting and the real part of the index of refraction from vacuum polarization. We can see that this is many orders of magnitude smaller than the vacuum polarization contribution.

The contribution to photon splitting from the total Coulomb field can be estimated from the transition rate W:[33]

$$W \approx 0.07\alpha^3\left(\frac{E_\gamma}{m_ec^2}\right)^4\left(\frac{E_{max}}{\sqrt{4\pi}E_S}\right)^6 |k|, \tag{21}$$

where $|k|$ is the wavenumber of the gamma ray and we have assumed the maximum value where the electric field is E_{max} and the photon is propagating perpendicular to it. For our parameter values, the shortest mean free path $1/W$ is of the order of 4000 cm for the highest photon energies of 60 MeV that we consider. Given that the size of the region we are considering is of micrometer order, this can be considered to be a small effect.

Within the scope of the processes we have considered, it can be seen that the vacuum polarization contribution to the index of refraction is at least two orders of magnitude larger than the imaginary contributions.

E. Possible application

As is apparent from the results in Fig. 3, the imploding microbubble has advantages over conventional materials in terms of the index of refraction. It dominates other processes at high photon energies and is independent of the photon energy as long as the

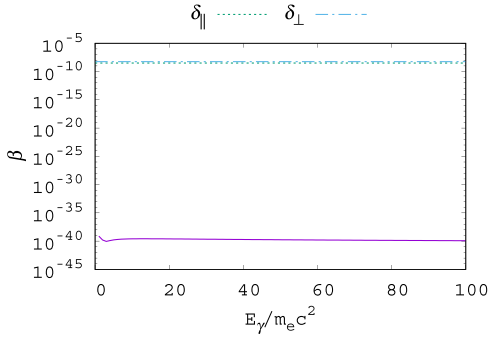

FIG. 5. Absolute value of the imaginary part of the index of refraction, $\beta(E_\gamma)$, obtained using values of σ_{unscr} from Ref. 32, vs normalized photon energy E_γ/m_ec^2. The real parts of the index of refraction, $\delta = n - 1$, due to vacuum polarization ($\delta_\parallel$ and $\delta_\perp$) are also plotted for comparison.

parameter ξ is small, which for our parameter values corresponds to photon energies below 60 MeV. Therefore, there is little chromatic aberration. The strongest lensing of gamma rays would be over the time scale for the existence of the peak fields (<0.1–0.01 fs). For very-short-duration focusing, micro-bubble implosions modifying vacuum polarization could be used as components of a transient lens, if arranged appropriately.

IV. CONCLUSION

We have shown the possibility of probing vacuum polarization in QED with micro-bubble implosions induced by ultra-high intensity lasers interacting with pre-formed targets. The effective field strength produced by a micro-bubble implosion is expected to reach 0.5% of the Schwinger-limit field strength with existing or upcoming high-intensity lasers. We have estimated the degree of bending of gamma rays as a function of the impact parameter with respect to the center of the micro-bubble from the deflection angle of light by vacuum polarization due to a spherically charged object previously derived in the Heisenberg–Euler formalism in Ref. 16. We have determined the necessary angular resolution to observe the bending of gamma rays passing by the micro-bubble. Changes in gamma-ray trajectories at sub-nanoradian resolution can be identified using existing devices.[17]

We have evaluated the contributions to the index of refraction from possible background processes. These processes contribute to both the real and imaginary parts of the index. One of the dominant contributions to the real part is the cold plasma effect. Although plasma effects are expected to occur, they are estimated to be smaller than the vacuum contribution for photon energies above a few hundred kiloelectron volts for a cold plasma and even smaller for a relativistically hot plasma. Other contributions such as nuclear Thomson and Delbrück scattering turn out to make larger contributions than the plasma; however, even their effects are small at photon energies of tens of megaelectron volts. We have estimated the imaginary part of the index of refraction due to absorptive processes and found that, for the processes we have considered, its contribution is at least two orders of magnitude smaller than that of the real part due to vacuum polarization at photon energies of 10 MeV and above. The imaginary part of the index of refraction due to background processes has also been evaluated. The dominant contribution is pair production in the atomic nuclear field, but this process can be experimentally discriminated from the scattered gamma-ray signal at the detector by means of the charge state of the exiting particles. On the other hand, the effect of Compton scattering cannot be distinguished from the signal resulting from vacuum polarization, but, for the photon energies we are considering, this contribution is nearly six orders of magnitude smaller than the signal. In conclusion, the index of refraction due to vacuum polarization is significantly higher than that due to any background process.

In addition to high-flux laser Compton scattering gamma-ray sources such as ELI-NP-GBS,[34] other transient high-power gamma-ray sources that could be used to measure and check the focusing include those based on ultrashort-pulse laser–plasma interactions (see, e.g., Refs. 35 and 36). Given that the index of refraction due to vacuum polarization can dominate other processes and is independent of photon energy at photon energies below 60 MeV for our parameter values, there could be advantages to the use of vacuum polarization via micro-bubble implosion as a transient lens. In addition, measurement of vacuum polarization via micro-bubble implosion would provide a test of the predictions of QED, with deviations indicating a likely need for new physics.

In this paper, we have only estimated the absorptive parts of the index of refraction. The actual technical details of how the small deflections involved could be measured have not been addressed, although a simple-minded approach would be to image highly collimated gamma rays before, at the peak of, and after compression, in a manner similar to how gravitational deflections of starlight (albeit in the visible range) are observed.[37] Additional factors to be considered with regard to experimental realization and the feasibility of measurement include (1) alignment, focusing the gamma rays down to scales less than 100 nm and measuring nanoradian to sub-milliradian deflections in a GAMS6 type of configuration,[17] (2) timing and synchronization of a sufficient number of gamma rays for detection with the implosion on femtosecond time scales, and (3) asymmetries, which reduce the maximum field and resulting scattering angles. An additional caveat is the upper limit of 60 MeV on the photon energy. High-energy electrons are produced in the interaction and could produce gamma rays by collisions with the incoming gamma rays or by other processes. These gamma rays colliding with the incoming gamma rays could produce electron–positron pairs, which would be an additional factor requiring consideration. These aspects are beyond the scope of this paper and, along with the possibility of using micro-bubble implosions as gamma-ray lenses, require further investigation.

ACKNOWLEDGMENTS

J. K. Koga acknowledges fruitful discussions with S. V. Bulanov and T. Hayakawa. A. V. Arefiev was supported by U.S. Air Force Project AFOSR No. FA9550-17-1-0382. Y. Nakamiya was supported by the Extreme Light Infrastructure Nuclear Physics (ELI-NP) Phase II, a project co-financed by the Romanian Government and the European Union through the European Regional Development Fund—the Competitiveness Operational Programme (1/07.07.2016, COP, ID 1334).

REFERENCES

[1]B. L. Garrec, S. Sebban, D. Margarone, M. Precek, S. Weber, O. Klimo, G. Korn, and B. Rus, "ELI-beamlines: Extreme light infrastructure science and technology with ultra-intense lasers," Proc. SPIE **8962**, 89620I (2014).

[2]S. Gales, K. A. Tanaka, D. L. Balabanski, F. Negoita, D. Stutman, O. Tesileanu, C. A. Ur, D. Ursescu, I. Andrei, S. Ataman, M. O. Cernaianu, L. D'Alessi, I. Dancus, B. Diaconescu, N. Djourelov, D. Filipescu, P. Ghenuche, D. G. Ghita, C. Matei, K. Seto, M. Zeng, and N. V. Zamfir, "The extreme light infrastructure—nuclear physics (ELI-NP) facility: New horizons in physics with 10 PW ultra-intense lasers and 20 MeV brilliant gamma beams," Rep. Prog. Phys. **81**(9), 094301 (2018).

[3]B. Shen, Z. Bu, J. Xu, T. Xu, L. Ji, R. Li, and Z. Xu, "Exploring vacuum birefringence based on a 100 PW laser and an x-ray free electron laser beam," Plasma Phys. Controlled Fusion **60**(4), 044002 (2018).

[4]A. Di Piazza, C. Müller, K. Z. Hatsagortsyan, and C. H. Keitel, "Extremely high-intensity laser interactions with fundamental quantum systems," Rev. Mod. Phys. **84**, 1177–1228 (2012).

[5]A. Milstein and M. Schumacher, "Present status of Delbrück scattering," Phys. Rep. **243**(4), 183–214 (1994).

[6]M. Schumacher, "Delbrück scattering," Radiat. Phys. Chem. **56**(1), 101–111 (1999).

[7]W. Greiner, B. Müller, and J. Rafelski, *Evolution of the Vacuum State in Supercritical Potentials* (Springer, Berlin, Heidelberg, 1985), Chap. 10, pp. 257–299.
[8]U. D. Jentschura, H. Gies, S. R. Valluri, D. R. Lamm, and E. J. Weniger, "Qed effective action revisited," Can. J. Phys. **80**(3), 267–284 (2002).
[9]F. Karbstein, "Photon polarization tensor in a homogeneous magnetic or electric field," Phys. Rev. D **88**, 085033 (2013).
[10]M. Murakami, A. Arefiev, and M. A. Zosa, "Generation of ultrahigh field by micro-bubble implosion," Sci. Rep. **8**(1), 7537 (2018).
[11]F. Sauter, "Über das verhalten eines elektrons im homogenen elektrischen feld nach der relativistischen theorie Diracs," Z. Phys. **69**(11), 742–764 (1931).
[12]W. Heisenberg and H. Euler, "Folgerungen aus der diracschen theorie des positrons," Z. Phys. **98**(11), 714–732 (1936).
[13]J. Schwinger, "On gauge invariance and vacuum polarization," Phys. Rev. **82**, 664–679 (1951).
[14]J. Y. Kim and T. Lee, "Light bending by nonlinear electrodynamics under strong electric and magnetic field," J. Cosmol. Astropart. Phys. **2011**(11), 017.
[15]W.-y. Tsai and T. Erber, "Propagation of photons in homogeneous magnetic fields: Index of refraction," Phys. Rev. D **12**, 1132–1137 (1975).
[16]J. Y. Kim and T. Lee, "Light bending in a coulombic field," Mod. Phys. Lett. A **26**(20), 1481–1485 (2011).
[17]M. M. Günther, A. V. Volotka, M. Jentschel, S. Fritzsche, T. Stöhlker, P. G. Thirolf, and M. Zepf, "Dispersive refraction of different light to heavy materials at MeV γ-ray energies," Phys. Rev. A **97**, 063843 (2018).
[18]T. Lee, "Bending of light in a coulomb gas," Phys. Rev. A **98**, 033811 (2018).
[19]V. N. Baĭer, A. I. Mil'shteĭn, and V. M. Strakhovenko, "Interaction between a photon and an intense electromagnetic wave," JETP **42**(6), 961–965 (1975), http://www.jetp.ac.ru/cgi-bin/dn/e 042 06 0961.pdf.
[20]S. L. Adler, "Photon splitting and photon dispersion in a strong magnetic field," Ann. Phys. **67**(2), 599–647 (1971).
[21]T. Heinzl and O. Schröder, "Large orders in strong-field qed," J. Phys. A: Math. Gen. **39**(37), 11623 (2006).
[22]D. J. Stark, C. Bhattacharjee, A. V. Arefiev, T. Toncian, R. D. Hazeltine, and S. M. Mahajan, "Relativistic plasma polarizer: Impact of temperature anisotropy on relativistic transparency," Phys. Rev. Lett. **115**, 025002 (2015).
[23]A. Arefiev, D. J. Stark, T. Toncian, and M. Murakami, "Relativistic effects in laser plasmas-plasma birefringence and generation of mega-tesla magnetic field," J. Plasma Fusion Res. **93**(11), 535–544 (2017) (in Japanese).
[24]P. Kane, L. Kissel, R. Pratt, and S. Roy, "Elastic scattering of γ-rays and x-rays by atoms," Phys. Rep. **140**(2), 75–159 (1986).
[25]T. Ericson and J. Hüfner, "Low-frequency photon scattering by nuclei," Nucl. Phys. B **57**(2), 604–616 (1973).
[26]R. Solberg, K. Mork, and I. Øverbø, "Coulomb and screening corrections to delbrück forward scattering," Phys. Rev. A **51**, 359–362 (1995).
[27]J. J. Klein and B. P. Nigam, "Dichroism of the vacuum," Phys. Rev. **136**, B1540–B1542 (1964).
[28]R. Battesti and C. Rizzo, "Magnetic and electric properties of a quantum vacuum," Rep. Prog. Phys. **76**(1), 016401 (2013).
[29]J. S. Heyl and L. Hernquist, "Birefringence and dichroism of the QED vacuum," J. Phys. A: Math. Gen **30**(18), 6485 (1997).
[30]M. Berger, J. Hubbell, S. Seltzer, J. Chang, J. Coursey, R. Sukumar, D. Zucker, and K. Olsen, XCOM: Photon Cross Section Database (version 1.5), URL: http://physics.nist.gov/xcom.
[31]J. H. Hubbell, H. A. Gimm, and I. Øverbø, "Pair, triplet, and total atomic cross sections (and mass attenuation coefficients) for 1 MeV-100 GeV photons in elements Z = 1 to 100," J. Phys. Chem. Ref. Data **9**(4), 1023–1148 (1980).
[32]A. M. Johannessen, K. J. Mork, and I. Øverbø, "Photon-splitting cross sections," Phys. Rev. D **22**, 1051–1061 (1980).
[33]Z. Bialynicka-Birula and I. Bialynicki-Birula, "Nonlinear effects in quantum electrodynamics. Photon propagation and photon splitting in an external field," Phys. Rev. D **2**, 2341–2345 (1970).
[34]K. Dupraz, K. Cassou, N. Delerue, P. Fichot, A. Martens, A. Stocchi, A. Variola, F. Zomer, A. Courjaud, E. Mottay, F. Druon, G. Gatti, A. Ghigo, T. Hovsepian, J. Y. Riou, F. Wang, A. C. Mueller, L. Palumbo, L. Serafini, and P. Tomassini, "Design and optimization of a highly efficient optical multipass system for γ-ray beam production from electron laser beam compton scattering," Phys. Rev. Spec. Top.–Accel. Beams **17**, 033501 (2014).
[35]T. Nakamura, J. K. Koga, T. Z. Esirkepov, M. Kando, G. Korn, and S. V. Bulanov, "High-power γ-ray flash generation in ultraintense laser-plasma interactions," Phys. Rev. Lett. **108**, 195001 (2012).
[36]D. J. Stark, T. Toncian, and A. V. Arefiev, "Enhanced multi-MeV photon emission by a laser-driven electron beam in a self-generated magnetic field," Phys. Rev. Lett. **116**, 185003 (2016).
[37]D. G. Bruns, "Gravitational starlight deflection measurements during the 21 August 2017 total solar eclipse," Classical Quantum Gravity **35**(7), 075009 (2018).